Static Response and Failure Prediction of Anisotropic Material Extrusion Polymer Parts

Jiahao Lu

A dissertation
submitted in partial fulfillment of the
requirements for the degree of

Master of Science in Aeronautics & Astronautics

University of Washington

2024

Reading Committee:

Marco Salviato, Chair

Richard Wiebe

Program Authorized to Offer Degree:
Aeronautics & Astronautics

University of Washington

Abstract

Static Response and Failure Prediction of Anisotropic Material Extrusion Polymer Parts

Jiahao Lu

Chair of the Supervisory Committee:
Associate Professor Marco Salviato
Aeronautics & Astronautics

The integration of additive manufacturing techniques has redefined the landscape of component manufacture, offering cost-effective and efficient alternatives to conventional manufacturing methods. This study delves into the application of an affordable MEx(Material Extrusion) 3D printer for producing PEEK (Poly-Ether-Ether-Ketone) polymer specimens designed for mechanical testing. The central aim is to investigate the feasibility of replacing non-structural metal aircraft components with MEx 3D printed PEEK counterparts.

The major advantage of MEx 3D printing lies in its ability to manufacture complex components without the need for molds or casts, leading to substantial cost reductions and accelerated development timelines. However, the inherent anisotropic nature of MEx-produced components poses a challenge. The layer-wise filament deposition gives inter-layer air gaps, introducing mechanical variability across different axes.

To address this challenge, our research employs a novel approach by subjecting MEx printed PEEK polymer specimen to mechanical tests involving forces applied at oriented angles to the anisotropic layer. This testing method is pivotal in modeling potential split and rupture of the MEx components, as encountered in real-world aircraft applications. By utilizing the Digital Image Correlation (DIC) tool to analyze full-field strain measurements and capture the elastic mechanical response of PEEK polymer specimen, our study establishes a strain-based failure criterion that defines the critical strain failure boundary.

TABLE OF CONTENTS

LIST OF FIGURES

GLOSSARY

PEEK: Poly-Ether-Ether-Ketone

PEKK: Poly-Ether-Ketone-Ketone

PAEK: Polyaryle-Ether-Ketone

MEX: Material Extrusion

DIC: Digital Image Correlation

FEA: Finite Element Analysis

UTS: Ultimate Tensile Strength

ACKNOWLEDGMENTS

I would like to express my deepest gratitude to my faculty advisors, Prof. Marco Salviato and Prof. Richard Wiebe, for their invaluable guidance and the exceptional opportunity to work on the BARC (Boeing Advanced Research Center) project that many dreamed of having. Years ago, I could not have imagined the chance to work closely with Boeing engineers.

A special thank you to Boeing fellow Eric Moyer for conceptualizing this remarkable project. I also extend my thanks to the members of the MAMS (Multi-scale Analysis of Materials & Structures) team, particularly Troy Nagakawa, Sean Phenisee, Antonio Deleo, Genki Masubara, Kush Dwivedi, and mostly importantly Chengjia Chen. I am exceptionally grateful to my PEEK teammates, Grace Dojan, Zhihao Meng, and Chester Pan, for their responsibility and positivity in our collaboration.

I would also like to thank UW staff members Kameron Harmon, who taught me how to use the ZUND ultrasonic router, and Bill Kuykendall, who instructed me on the INSTRON load frame. Each of these individuals is the key in my success, and I am thankful to have had their support.

Finally, I extend my heartfelt thanks to my parents for their emotional and financial support over the past 24 years. They have always stood by my side, shielding me from life's challenges. They are the world's best parents, period.

Chapter 1

INTRODUCTION

1.1 Introduction of 3D printed high performance thermoplastic

3D printing high performance thermoplastic technology is unlike the conventional 3D printing tech[10]. Printing such high-temperature resistance, and excellent chemical resistance material means that a 3D printer with robust heating and insulating capability is required. FUNMAT-HT 3D printer(Fig 1.1) [8] was chosen which is the relatively cheap in the market though remains as a quality 3D printer. The High performance thermoplastic family our research focuses on falls under the PAEK(Polyaryle-Ether-Ketone)[15] family which consists PEEK, PEI, PEKK, PEKEKK, etc. In specific to this research PEEK, also known as Poly-Ether-Ether-Ketone, as one the widely used high performance polymer is used as the filament of FUNMAT-HT 3D printer. In order to constantly extrude the PEEK filament out of the printer nozzle, the nozzle needs to be heated at $\approx$ 440 degree Celsius where the conventional 3D printer nozzle only needs $\approx$ 160 degree Celsius. At this closed cabin 3D printer, chamber is heated and maintained at 85 degree Celsius and printer bed is kept at 145 degree Celsius. All these feature are the key requirement to receive quality printing parts that conventional 3D printer do not need. There are two types of crystallinity appearance on PEEK, semi-crystalline which is high crystallinity and amorphous which is low crystallinity shown in Fig 1.2. It is know from previous studies [9], the lower the cooling rate of the extruded filament, the higher the crystallinity of PEEK component produced, thence better mechanical performance. Lower cooling rate allows the fiber chain to be closely packed and ordered, where a high cooling rate has randomly ordered fiber chain which permits gap and transparency seen as amorphous appearance. Altering the temperature settings and printing speed can allow one to achieve the desired crystallinity. In this research, a consistent temperature setting and printing speed is determined which ensures the printed components has consistent crystallinity for our study.

There is annealing method which evens the crystallinity of PEEK across the geometry, however the printed PEEK geometry would introduce residual stress and bending moment caused by the heat source which is not included in the interest of this research.

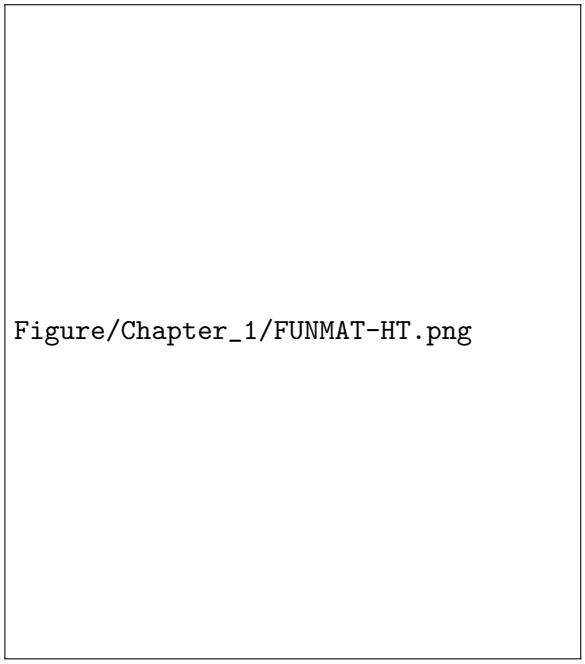

Figure 1.1: FUNMAT-HT 3D printer [8]

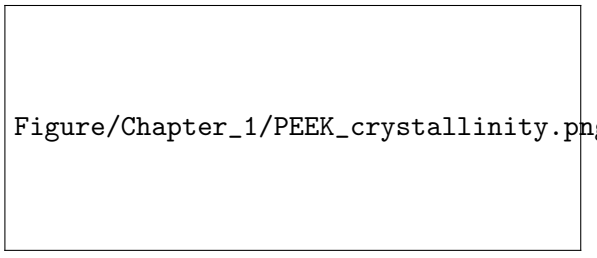

Figure 1.2: PEEK Crystallinity [1]

1.2 Motivation and objectives

The high performance PEEK polymer has been extensively used in aerospace applications, but 3D printed PEEK has not seen similar adoption. Currently, 3D printed PEEK remains hesitant to the aerospace industry. The advantages of 3D printing polymer over injection molding are significant. In the field of small scale manufacturing, 3D printer can rapidly transition components from design stage to manufacturing stage, offering greater economic efficient comparing to injection molding. In terms of design flexibility, 3D printed components can be redesigned in more optimal way. Often, the optimal redesigning improves the stiffness of the component and reduces overall weight significantly. This a critical consideration in the aerospace industry where every gram matters. The image 1.3 by Hexcel provides more insight in these advantages. However, challenges arise due to the inherent anisotropy of 3D printed polymers, which results in unpredictable failure mechanism. This research aim to understand the anisotropy by investigating the fiber and layer interaction under applied loads, achieved by orientating the fiber alignment at various angles. Additionally, this research also seeks to obtain the mechanical property of 3D printed PEEK by design and test a specific type of dogbone specimen. Lastly, the research aims to predict the failure mechanism using strain based failure criteria through direct strain measurement with Digital Image Correlation (DIC) technique. The ultimate goal is to enhance predictability of 3D printed PEEK, making it a safer option for aerospace applications.

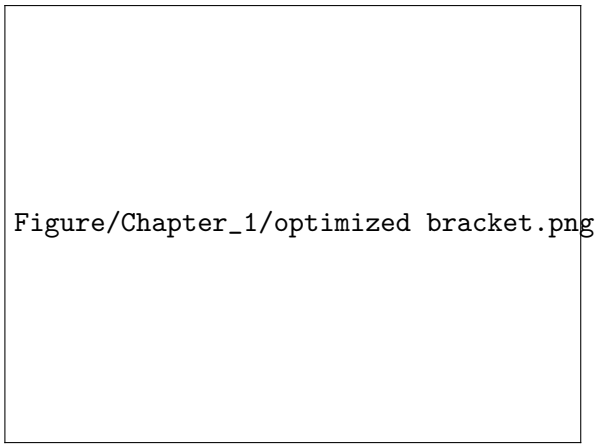

Figure 1.3: Optimized Bracket [11]

Chapter 2

THEORY AND METHODOLOGY

2.1 Background of 3D Printing

The Material Extrusion (MEx) 3D printer operates with a nozzle traversing the x and y axes, while the build plate ascends along the z-axis, enabling the gradual buildup of filament layer by layer shown in Fig 2.1. The bonding process involves heating the filament to a liquid state, followed by rapid solidification to integrate with the preceding layer. However, complete bonding between layers remains elusive, resulting in inherent anisotropy and weakened inter-layer cohesion in the printed object. This underscores the significance of the ongoing research. Regarding x-y axis movement, various nozzle configurations exist to fill each layer, with the most common being 0/90 and ± 45 configuration. This research aims to explore both raster configurations as illustrated in Fig 2.2. Both configurations are common tool path in the industry. Each potentially offer distinct advantages than the other.

2.2 Specimen Design

A specific dogbone dimension is designed for the test specimen shown in Table 2.1. To observe the interaction between layer-to-layer bonding, a wide strain gauge is necessary. The radius of the tapered edges is proportionate to the intentionally fixed value of 30mm width gauge, referencing the D638 type I dogbone[2], while maintaining a 20mm gauge length. However, due to the limitations of the 3D printer, extending the grip section and gauge length is unfeasible without compromising the gauge width. The edges are tapered to enforce failure initiation within the gauge length. The stress concentration on the taper radius was validated to be between 1.01 to 1.02 using an isotropic FEA module, as depicted in Figure 2.3. The maximum Von-Mises Stress is shown as 60.56 MPa where the 5000 Newtons of load apply is applied over the surface area of 84 mm$\wedge$2 (30mm x 2.8mm).

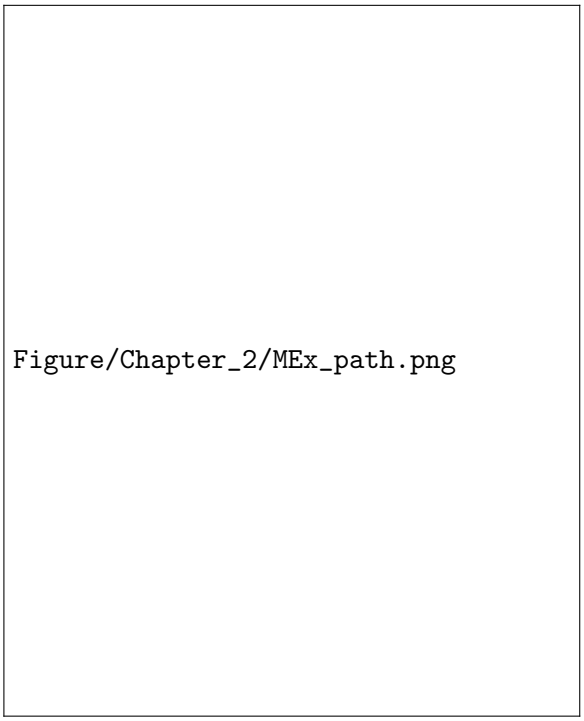

Figure 2.1: MEx [5]

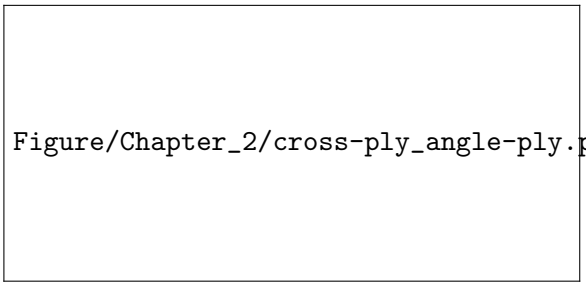

Figure 2.2: a) ±45 b) 0/90 [12]

Nominal Stress = Force Applied / Surface Area = 59.52 MPa. Hence, Stress Concentration = Maximum Stress / Nominal Stress = 1.017 is within acceptable range.

In addition at ensuring the stress concentration is away from the grip, both sides and ends of the specimen grip are epoxy glued with 0.093" fiber glass plate added to a total of ≈7.52mm thick dogbone coupon Fig 2.4. This method also reduces the indentation damage

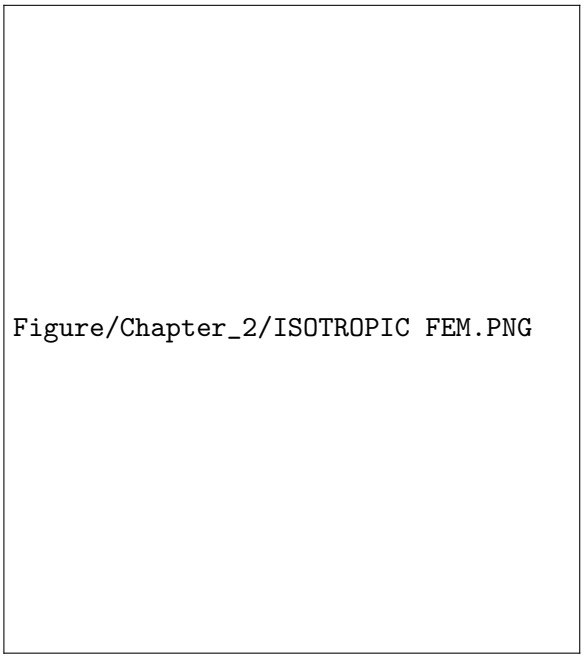

Figure 2.3: Isotropic FEM Von-Mises Max Stress

by load frame jaw during pre-load stage. The fiber glass plate also mitigate slippage and breakage at grip.

In order gain deeper insights into the interaction of fiber and layer, the test specimen need to be printed at various angles relative to the printing bed. According to ASTM 52921[3], reorienting the dogbone around the y-axis is indicated by B = degrees of orientation. This study investigates B angles in 0, 15, 30, 45, 90 degrees, with B = 0 representing the specimen with the most fiber dominant angle and B = 90 representing a specimen entirely sustain load by layer-to-layer bonding shown in Fig 2.15. Instead of employing support structures to directly print the dogbone shape at an angle, sheets of 116 x 116 x 2.8 (mm) square blanks are printed in both 0/90 and ± 45 configurations shown in Fig 2.13. The size of blank is large enough to extract all types of B angles. Within each blank, B angle coupons are extracted using a CNC ultrasonic router, precisely cutting them to the exact dogbone dimensions as various B angles shown in the Fig 2.5. Dark tape along the edges of blank are used to constraint the blank during routing process.

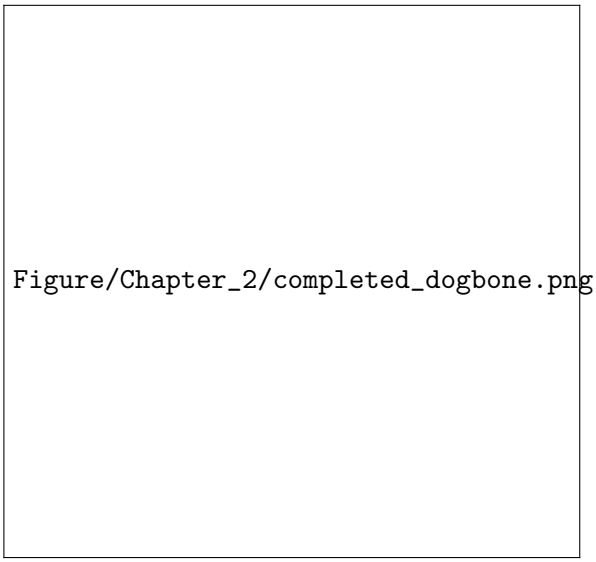

Figure 2.4: completed test specimen

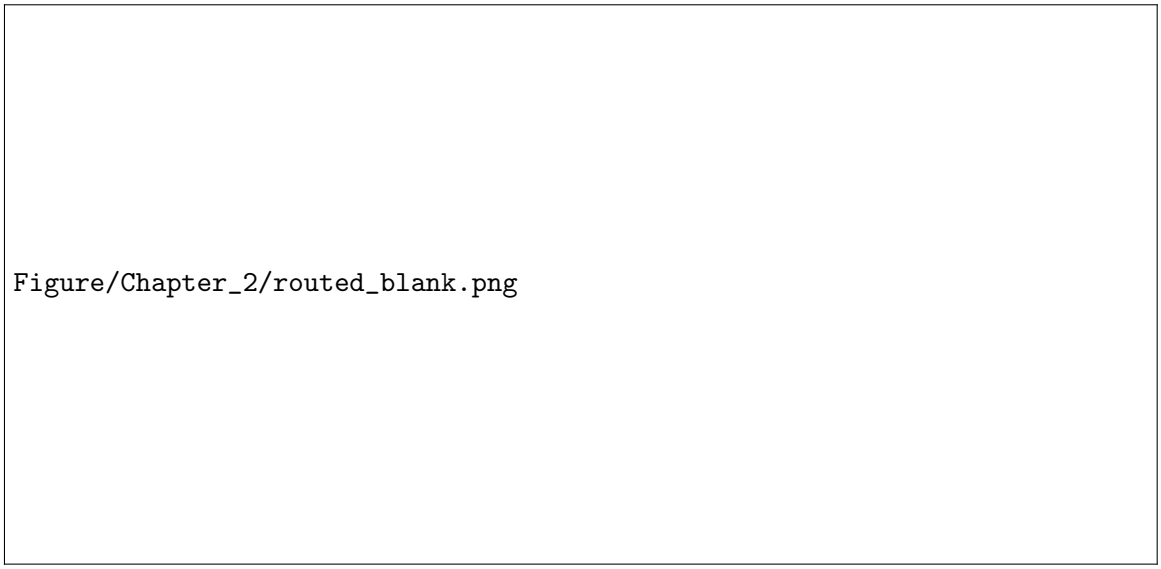

Figure 2.5: B=15 Dogbone manufactured by CNC Ultrasonic Router

To maintain the consistency of the 3D printer, traveler coupons are also prepared alongside the blanks. Two types of travelers are produced, both conforming to the D836 type V[2] dimension shown in Fig 2.7 and Table 2.1. Vertical Travelers are from the excess material

of the same blank used for the dogbone coupons. They are extracted at B = 90 and tested to ensure uniformity across the blanks. Additionally, for every three blanks manufactured, a flat blank is printed next to a blank on the printing bed shown in Fig 2.13. Subsequently, one flat traveler coupon is extracted from each flat blank using the CNC ultrasonic router.

	Dogbone Coupon	**Vertical(B=90) & Flat Traveler**
W—Width of narrow section	30	3.18
G-Gauge length	20	7.62
WO—Width overall	34	9.53
LO—Length overall	110	63.5
R—Radius of fillet	175	12
T-Thickness	2.8	2.8 & 3

Table 2.1: dogbone dimensions (mm)

2.3 Testing Theory

The mechanical tests conducted in this research focuses on tensile test. These tests aim at acquiring mechanical properties by solely applying force in the Y-direction. Consequently, there is no force applied on the free edges in the X and Z directions.

3D printed material is considered Transversely Isotropic [4] which is a subclass of Orthotropic. Transversely Isotropic material has same material property in the X-Z plane and different properties in directions normal to X-Z plane. The mechanical properties of Transversely Isotropic material are acquired by using Hooke's law[4] in compliance form shown in 2.6. There are 5 elastic constants needed in the Transversely Isotropic constitutive equation which are Young's modulus E_{11}, E_{22}; Poisson ratio ν_{12}, ν_{21}; and Shear modulus G_{12}. In the Plane Stress assumption [4] where the thickness of the plate in Z-direction is infinitely small compared to the X & Y directions, the in-plane stresses are zero ($\sigma_{33}, \sigma_{23}, \sigma_{31} = 0$). Hence, E_{33}, ν_{23}, ν_{32}, ν_{31}, ν_{13}, G_{23}, G_{31} are zero leaving only 5 elastic constants needed in our study. Note: $-\nu_{21}/E_{22} = -\nu_{12}/E_{11}$

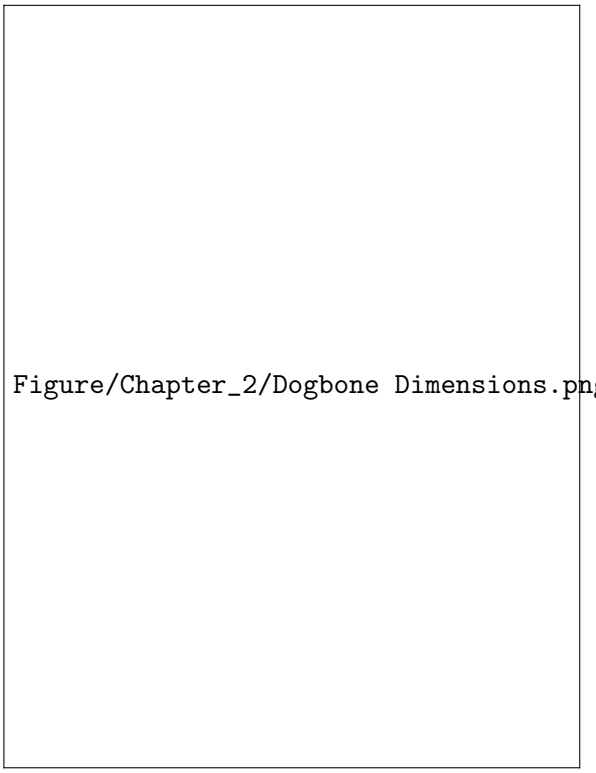

Figure 2.6: dogbone dimensions graphic

In order to determine these 5 unknown elastic constants experimentally, We use three B angle coupons to generate 5 equation based on compliance matrix with known initial conditions. B=0 coupon is only applied with stress σ_{22} where σ_{11} and σ_{33} are zero. Hence, E_{22}, ν_{21} are

$$E_{22} = \frac{\sigma_{22}}{\epsilon_{22}} \tag{2.1}$$

$$\nu_{21} = -\frac{\epsilon_{11}}{\epsilon_{22}} \tag{2.2}$$

B=90 coupon is only applied with stress σ_{11} where σ_{22} and $\sigma_3 3$ are zero. Hence, E_{11}, ν_{12} are

$$E_{11} = \frac{\sigma_{11}}{\epsilon_{11}} \tag{2.3}$$

$$\nu_{12} = -\frac{\epsilon_{22}}{\epsilon_{11}} \tag{2.4}$$

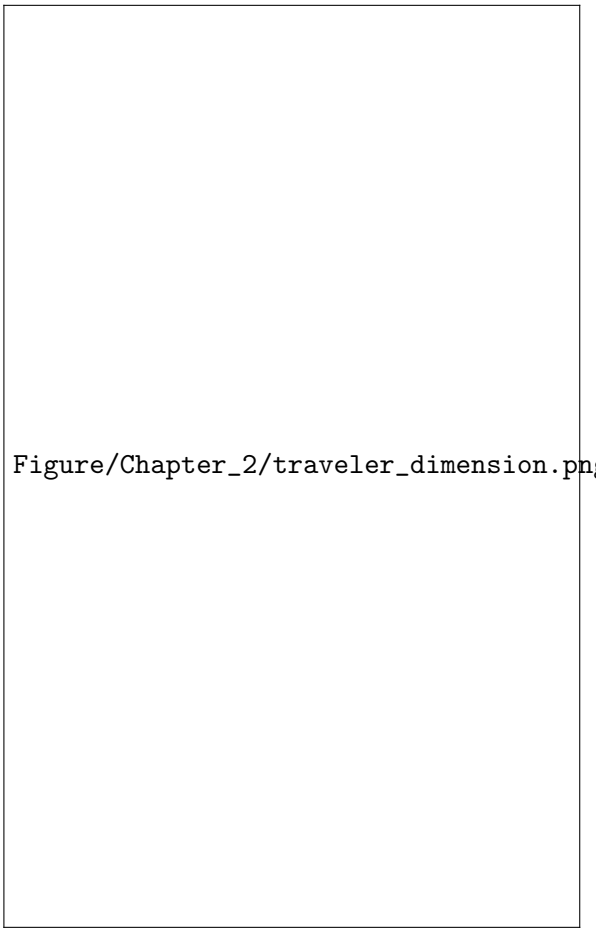

Figure 2.7: Traveler dimensions graphic

B=45 is only applied with stress σ_{12}, hence, G_{12} is

$$G_{12} = \frac{\sigma_{12}}{2\epsilon_{12}} \tag{2.5}$$

$$\begin{bmatrix} \epsilon_{11} \\ \epsilon_{22} \\ \cancel{\epsilon_{33}} \\ \cancel{\epsilon_{23}} \\ \cancel{\epsilon_{31}} \\ \epsilon_{12} \end{bmatrix} = \begin{bmatrix} \frac{1}{E_{11}} & -\frac{\nu_{21}}{E_{22}} & \cancel{-\frac{\nu_{31}}{E_{33}}} & 0 & 0 & 0 \\ -\frac{\nu_{12}}{E_{11}} & \frac{1}{E_{22}} & \cancel{-\frac{\nu_{32}}{E_{33}}} & 0 & 0 & 0 \\ \cancel{-\frac{\nu_{13}}{E_{11}}} & \cancel{-\frac{\nu_{23}}{E_{22}}} & \cancel{\frac{1}{E_{33}}} & 0 & 0 & 0 \\ 0 & 0 & 0 & \cancel{\frac{1}{2G_{23}}} & 0 & 0 \\ 0 & 0 & 0 & 0 & \cancel{\frac{1}{2G_{13}}} & 0 \\ 0 & 0 & 0 & 0 & 0 & \frac{1}{2G_{12}} \end{bmatrix} \begin{bmatrix} \sigma_{11} \\ \sigma_{22} \\ \cancel{\sigma_{33}} \\ \cancel{\sigma_{23}} \\ \cancel{\sigma_{31}} \\ \sigma_{12} \end{bmatrix} \tag{2.6}$$

The test specimens exhibit both brittle and ductile behavior, depending on the angle of orientation. Brittle behavior is likely to appears in specimens with larger B angles, where the weaker layer bears the majority of the force. Conversely, specimens with smaller B angles can display ductile behavior, as the load is predominantly exerted along the fiber direction. Specimens exhibiting greater ductility experience necking and yielding. Therefore, conversion from engineering stress and strain to true stress and strain is done for more accurate analysis.

2.4 DIC technique

The DIC (Digital Image Correlation) method represents a novel approach to obtain strain data through sequenced images. In contrast to extensometer method[7], which involves physically attaching two pins to the edge of the gauge length to measure strain shown in Fig 2.8, the DIC method operates without direct contact with the specimen. Instead, a thin film of adhesive tattoo paper, uniformly covered with laser printed speckle patterns, is applied to the entire visible specimen surface shown in Fig 2.4. A camera then captures high-resolution images of the specimen surface at a consistent rate (2frames/sec) during the tensile test shown in Fig 2.9.

These images, showing visible speckles, are cropped and converted to black and white via MATLAB code written by Troy Nakagawa to reduce file size. Subsequently, the images are processed using post-processing software, such as GOM correlate[16], which tracks the movement of every speckled dots in each frame and generates strain data for the entire specimen surface in both global(XYZ-directions) and local(123-direction) coordinate system. Local true strain data is obtained by rotating the principle axis from global coordinate system to the direction of printing layer within GOM correlate. Since the test specimen undergoes large deformation, true strain (Eq 2.7)is more appropriate than engineering strain. Finally, the local true strain data is plotted against local true stress data.

$$\epsilon_t = ln(1 + \delta L/L_0); \delta L = \text{change in length}, L_0 = \text{overall length} \tag{2.7}$$

Two specimens in each configuration were tested with mechanical extensometer along

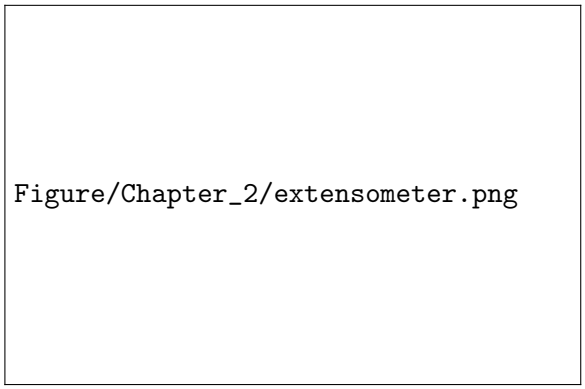

Figure 2.8: Extensometer (Instron) [7]

Figure 2.9: DIC setup

with DIC equipment both capturing the strain data simultaneously. From the stress and strain curves provided from both methods shown in Fig 2.10, it confirms the use of DIC method is valid.

The purpose of obtaining the local true stress and strain curve is to align the material's principle directions. The local coordinate system captures the directional dependence of material properties more accurately. The load frame outputs the load(in kN) in Y-direction, and true σ_{YY} is calculated by dividing the load by true cross-sectional area of gauge. True cross-sectional area is the true gauge width multiply by coupon thickness. For ductile specimens, true gauge width at each frame is obtained using distance measurement tool in GOM correlate. To compute true σ_{22} and σ_{11}, the stress date in the global coordinate system (X-Y-Z) must be transformed into a local coordinate system (1-2-3) using a rotational tensor[4] shown in Eq 2.8. Depending on the specimen's B angles, this tensor rotates the stress tensor to align with corresponding direction where the fiber dominance direction corresponds in the 2-direction and the filament layer aligns with the 1-direction.

2.5 Manufacturing

The FUNMAT HT 3D printer produces two types geometries, blanks and flat blanks dimensions are shown in Table 2.2. The printer uses a pre-set printing parameter for all blanks and flat blanks produced via Cura slicer[14]. The printer nozzle extrudes 0.4mm filament and prints at 0.1mm layer height in 0/90 & $\pm$45 configuration with no walls. The printing speed is set at 50mm/s throughout the manufacturing process unchanged. Filament infill is set at 100%, though porosity will be present due to natural of 3D printing. Blanks are printed vertically up and flat blanks are printed flat on the bed shown in Fig 2.13. The size of the blank is designed to extract one or two test specimens depending on the B angles. The plan is to produce 6 specimens from each configuration and B angles (B=0, 15, 30, 45, 90) summing up with a total of 50 blanks producing 60 test specimens along with 28 vertical travellers and 13 flat travellers. Graphics for specific B angle coupon are shown in Fig 2.15, parallel lines shown are the fiber layers. Vertical Travellers are extracted from the extra material available of the same blank producing specimens at B=90 angle shown in Fig 2.14. Flat Travellers are extracted from the flat blank shown in Fig 2.13 which has a fiber

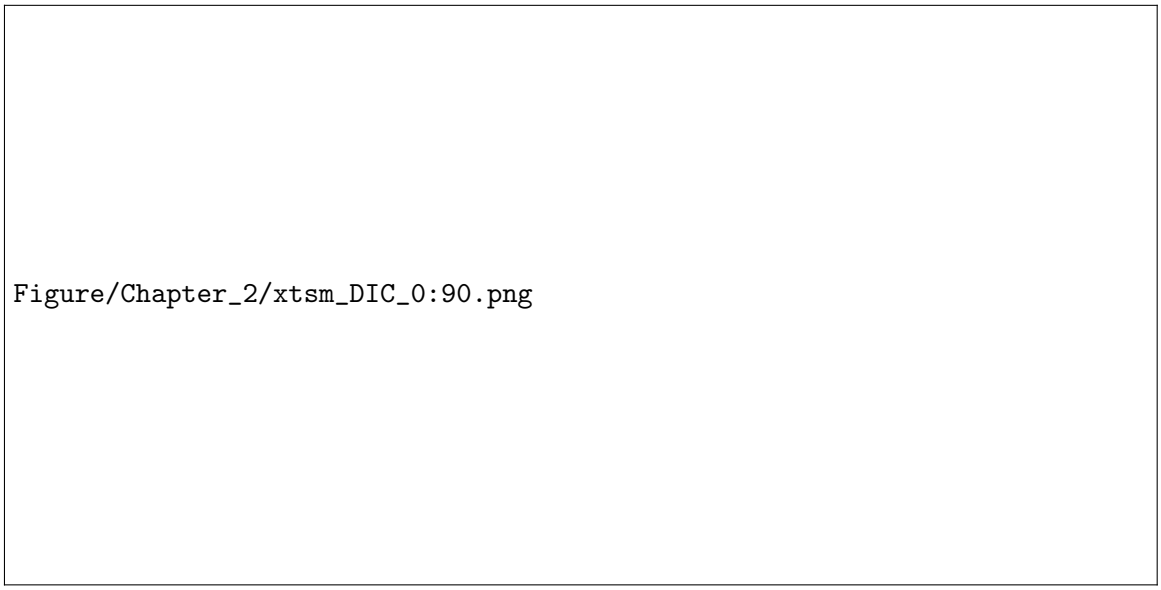

(a) extensometer vs DIC (0/90)

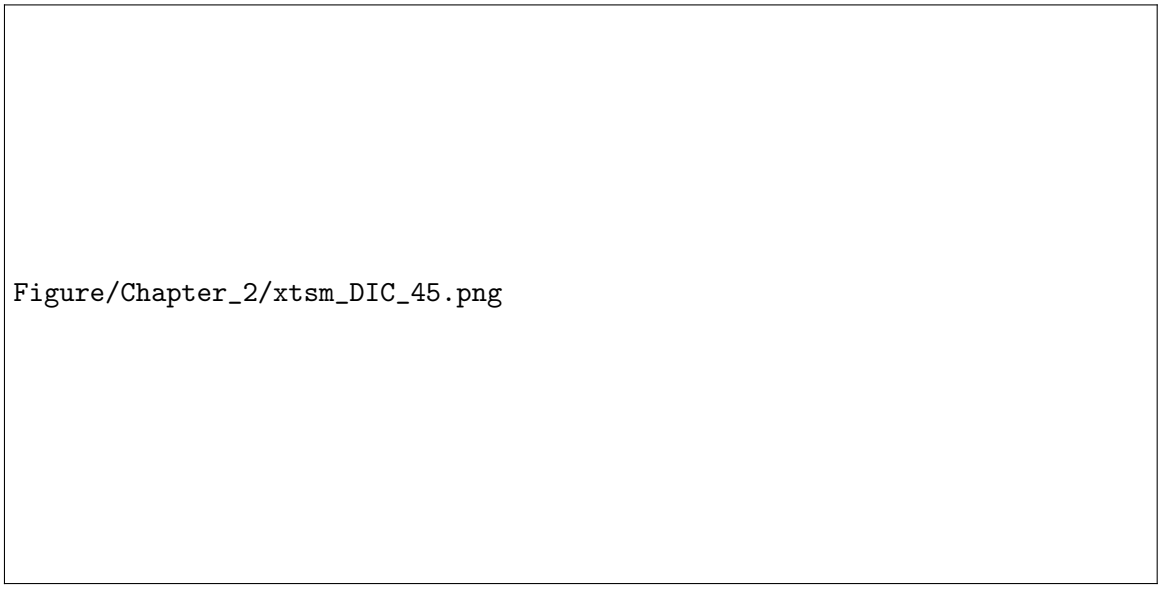

(b) extensometer vs DIC (±45)

Figure 2.10: Extensometer vs DIC Comparison

$$\begin{bmatrix} \sigma_{11} \\ \sigma_{22} \\ \sigma_{12} \end{bmatrix} = \begin{bmatrix} c^2 & s^2 & 2cs \\ s^2 & c^2 & -2cs \\ -cs & cs & c^2 - s^2 \end{bmatrix} \begin{bmatrix} \sigma_{xx} \\ \sigma_{yy} \\ \sigma_{xy} \end{bmatrix} \tag{2.8}$$

Figure 2.11: Rotational tensor, where $c = \cos\theta$ and $s = \sin\theta$

orientation of B=0 angle. (Note: A few vertical and flat travellers had defects and were thrown away) The cutting of the test specimens is done solely by the CNC ultrasonic router provided by ZUND[17] shown in Fig 2.5 and 2.12. The CNC Ultrasonic Router bit cuts the blank at 50000rpm, such high frequency focus energy on small area at the cutting edge which minimizes heat generation. Therefore, the edge of dogbone does not melt through the cutting process. After the test specimens are cut, glass fiber end tabs are applied on both ends and both sides. Speckled tattoo is then applied on the specimen surface for DIC. Then the test specimen manufacture is complete.

	blank	**flat blank**
Width	116	12
Length	116	64
Thickness	2.8	3

Table 2.2: geometry dimensions (mm)

Figure 2.12: ZUND ultrasonic router [17]

Figure 2.13: Blank & Flat Blank

Figure 2.14: B=45 coupon manufactured with Vertical Traveler along side

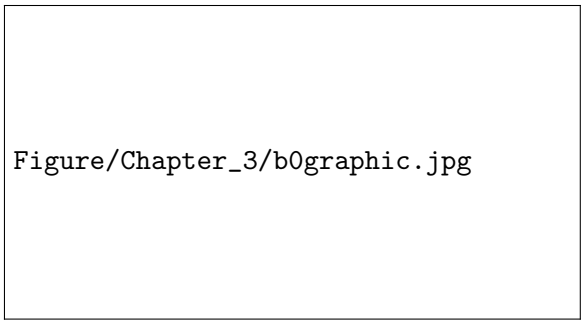

(a) B=0

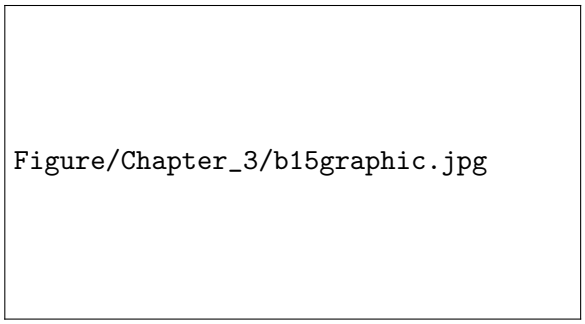

(b) B=15

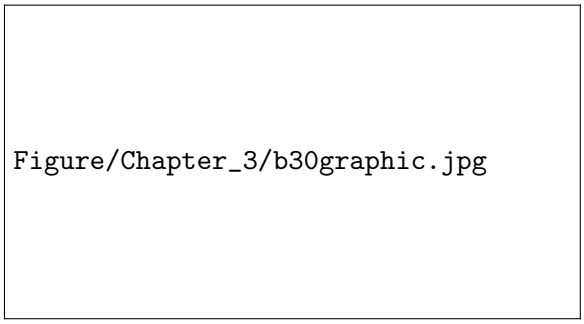

(c) B=30

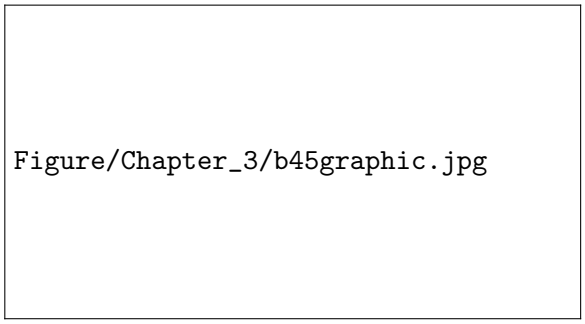

(d) B=45

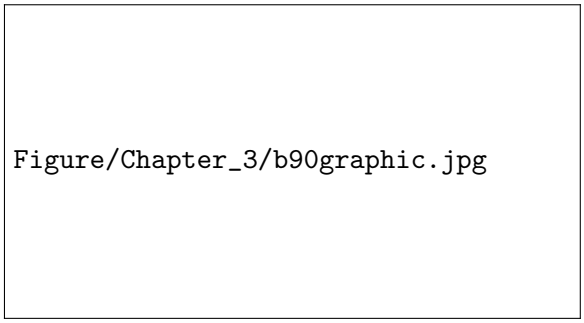

(e) B=90

Figure 2.15: B angle graphics. Image credit: [Grace Dojan]

Chapter 3

EXPERIMENTS

3.1 Experimental Setup

The tensile test was done with the hydraulic load frame provided by Shorewestern shown in Fig 3.2. Test specimens are place against alignment fixture on both end of the jaws that is pressure controlled at $\approx$ 300 psi. Speckled side is placed facing towards the camera for DIC. As the cross head begins to extend at constant displacement rate (cross-head speed) of 0.025mm/sec, camera is set to take interval shots at 2 frames/sec. The tensile load is also applied along the Y-axis.

The tensile test for the travelers was done with the ball screw load frame provided by Instron shown in Fig 3.1. Once both ends of the travelers are tighten, 5mm extensometer is pinned in between the gauge length. DIC was not used since the purpose was only to check the consistency of every prints.

3.2 Experimental Result

3.2.1 Coupon

After testing the dogbone coupon, load and displacement data along with DIC strain data obtained from camera are integrated. Stress and Strain data in global coordinate system is rotated into local coordinate system for further analysis. Figure 3.3 & 3.3 depict the local Stress vs. Strain curves for all tested B angles in both configurations. From these curves, the Ultimate Tensile Strength (UTS) & Fracture Strength results of both 0/90 & $\pm$45 configurations are obtained and averaged, as shown in Tables 3.1 and 3.2. Ultimate Tensile Strength (UTS) is represented by $\sigma_{UTS,22}$ & $\sigma_{UTS,11}$ for 2 & 1 directions. Fracture Strength is denoted by $\sigma_{f,22}$ & $\sigma_{f,11}$ for 2 & 1 direction. Fracture Strength differs from UTS particularly for ductile specimens that exhibit strain softening, hence B=0 and B=15 show Fracture Strength. The Coefficient of Variation(CV) in percentage is provided in the tables

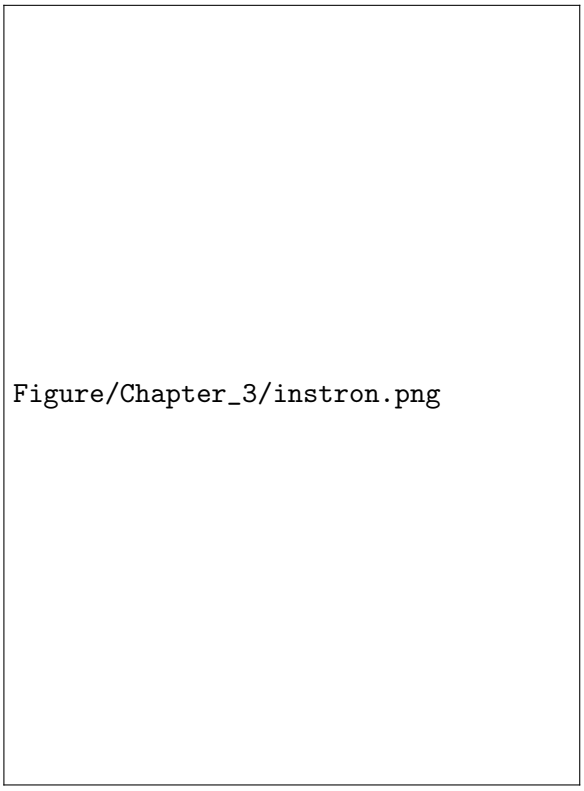

Figure 3.1: travelers on Instron load frame with extensometer [6]

to offer insights into data variability.

Table 3.3 presents the experimental results of five elastic constants obtained from the tensile tests conducted for both configurations . The Coefficient of Variation (CV) is also included to indicate data variability. These five elastic constants constitutes the stiffness matrix of the anisotropic 3D printed PEEK Polymer investigated in this study.

Fig 3.5 & Fig 3.6 show images of all 60 coupons at both configuration after completion of the tests. These images provides the location and direction of the fracture. The numbers written in black are the serial number for each coupon to keep track of the source in reference to test plan sheet (Fig A.1). Specimen 19, 20, 30 were replaced by 19R, 20R, 30R as the experiment were redone.

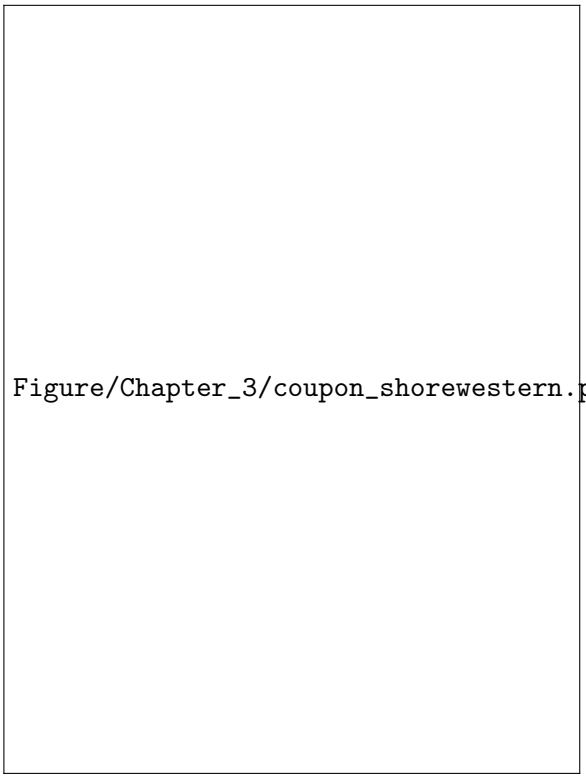

Figure 3.2: Coupon on Load Frame [13]

B angle	Number of Coupons Tested	$\sigma_{UTS,22}$ (MPa)	$\sigma_{UTS,11}$ (MPa)	$\sigma_{f,22}$ (MPa)	$\sigma_{f,11}$ (MPa)
0	6	92.68±0.63%	0	81.21±7.74%	0
15	6	55.08±17.55%	3.93±17.55%	–	–
30	6	36.15±6.34%	12.05±6.34%	–	–
45	6	20.82±12.34%	20.82±12.34%	–	–
90	6	0	25.11±10.55%	0	–

Table 3.1: Ultimate Tensile Strength & Fracture Strength of 0/90 configuration

3.2.2 Traveler Coupon

Among the twenty-eight vertical travelers shown in Fig 3.7a, eleven are configured as 0/90 and seventeen as ±45, all cut at B=90 angle. Figure 3.8a demonstrates the brittle behavior

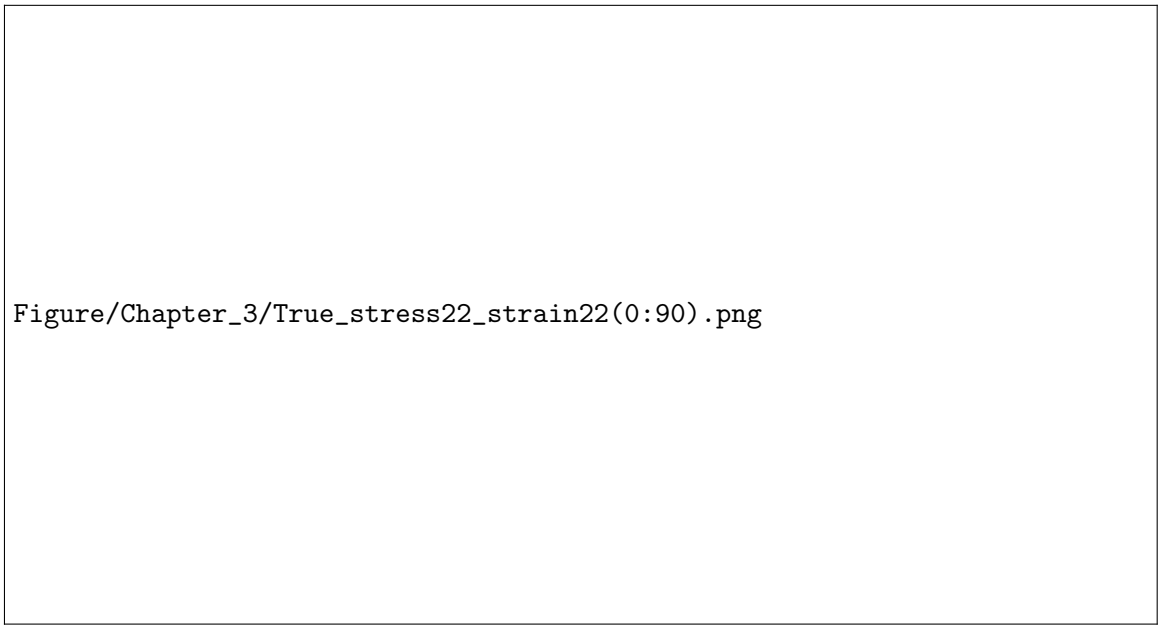

(a) σ_{22} vs $\epsilon_{22}(0/90)$

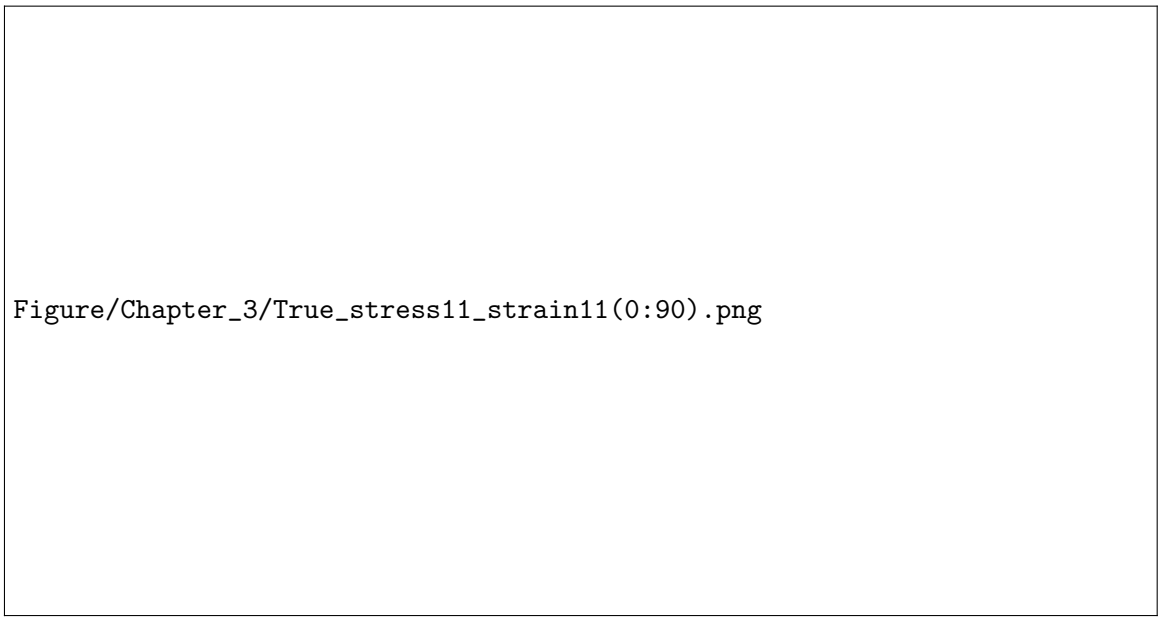

(b) σ_{11} vs $\epsilon_{11}(0/90)$

Figure 3.3: Stress vs Strain (0/90 configuration)

B angle	Number of Coupons Tested	$\sigma_{UTS,22}$ (MPa)	$\sigma_{UTS,11}$ (MPa)	$\sigma_{f,22}$ (MPa)	$\sigma_{f,11}$ (MPa)
0	6	88.82±2.23%	0	74.07±9.13%	0
15	6	80.98±2.29%	5.83±1.99%	70.87±7.43%	5.06±7.43%
30	6	58.65±4.57%	19.56±4.52%	–	–
45	6	29.51±7.16%	29.51±7.16%	–	–
90	6	0	31.16±13.28%	0	–

Table 3.2: Ultimate Tensile Strength & Fracture Strength of ±45 configuration

Configuration	E_{11} (MPa)	E_{22} (MPa)	G_{12} (MPa)	ν_{12}	ν_{21}
0/90	32.94±6.61%	31.29±1.7%	14.49±7.19%	0.35±6.62%	0.42±2.59%
±45	30.29±3.21%	26.07±7.57%	14.16±5.97%	0.37±4.29%	0.39±1.94%

Table 3.3: Material Properties of 0/90 & ±45 coupons

of all vertical travellers on stress-strain curve. The trend-line drawn confirms the consistency of the vertical travelers within the elastic region, indicating that the blank produced by 3D printer are of the acceptable quality.

From the thirteen flat travellers shown in Fig 3.7b, six are configured as 0/90 and seven as ±45. Figure 3.8b indicates all flat travellers exhibit ductile behavior. Although these flat travelers fracture at different loads, the slope within the elastic region remains consistent. Flat traveler #3 appears to have lower post peak than the others; however, its corresponding dogbone specimen (#9) has UTS of 31.6 MPa, which is close to the mean UTS of 29.5 MPa. This confirms that flat travelers also verify the printing quality of 3D printer. Therefore, further investigation into the dogbone specimen may be proceed.

(a) σ_{22} vs $\epsilon_{22}(\pm 45)$

(b) σ_{11} vs $\epsilon_{11}(\pm 45)$

Figure 3.4: Stress vs Strain (± 45 configuration)

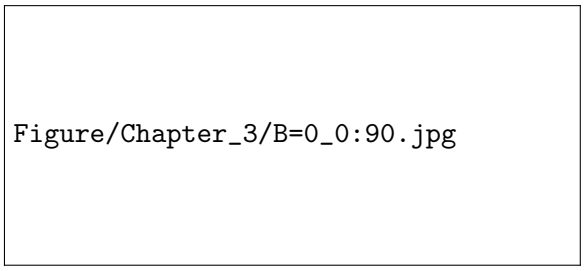

(a) B=0

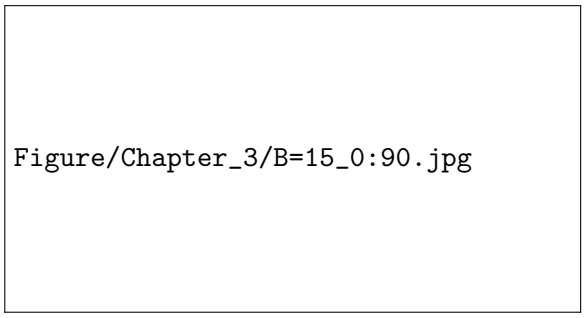

(b) B=15

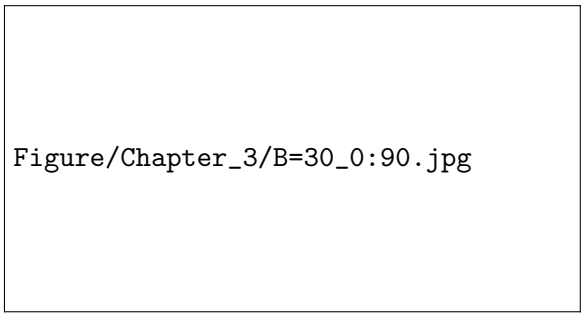

(c) B=30

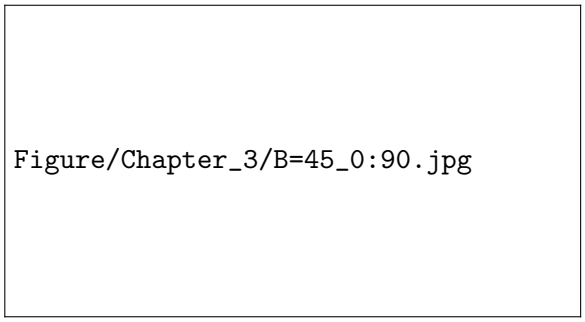

(d) B=45

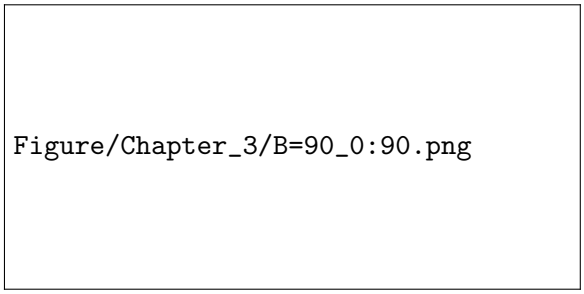

(e) B=90

Figure 3.5: All Tested Dogbone Coupon (0/90 configuration)

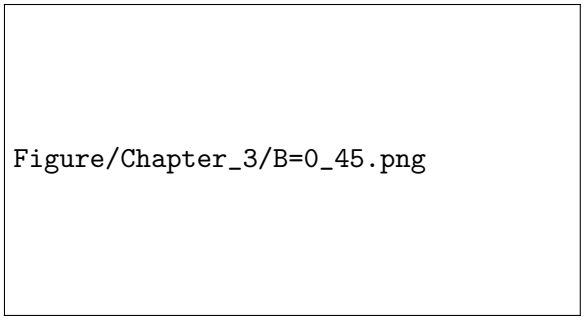

(a) B=0

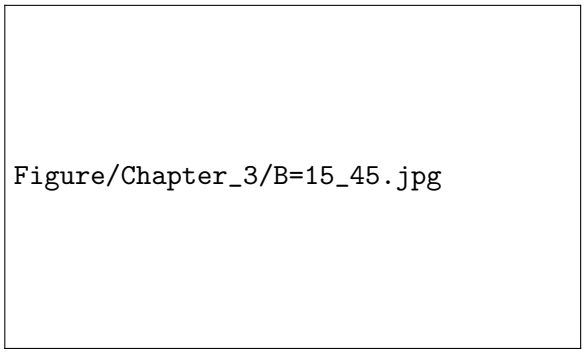

(b) B=15

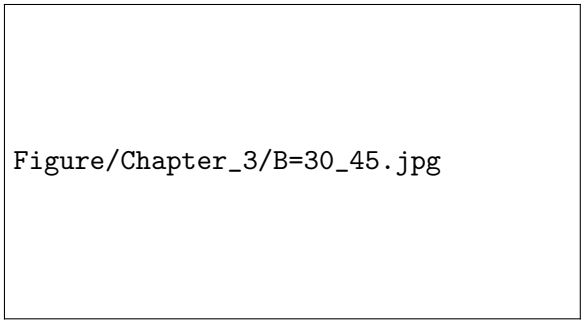

(c) B=30

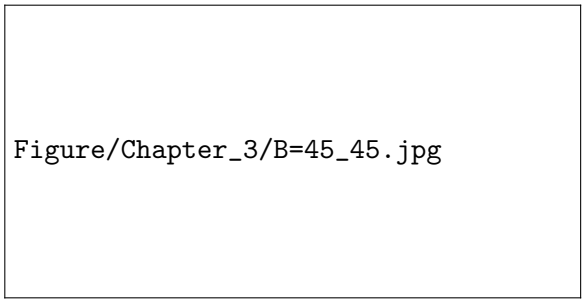

(d) B=45

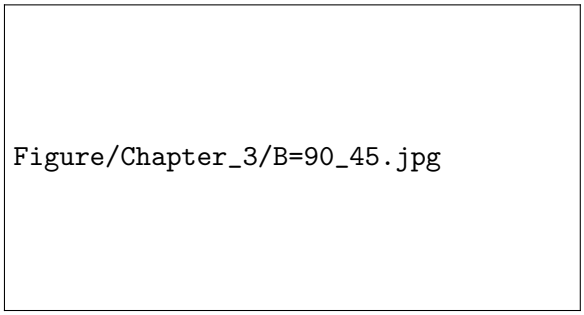

(e) B=90

Figure 3.6: All Tested Dogbone Coupon (±45 configuration)

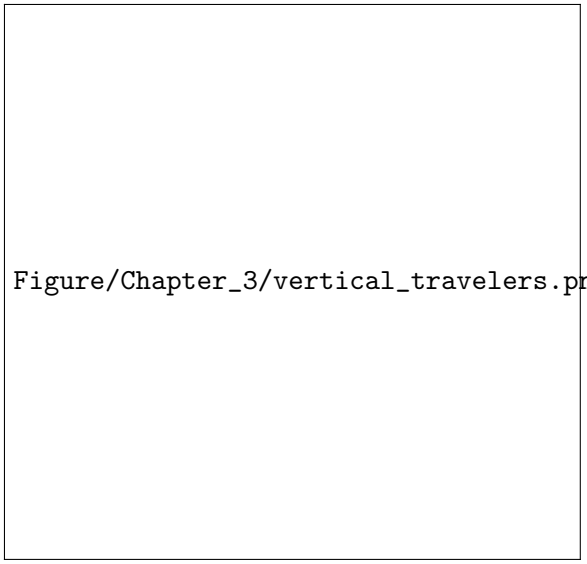

(a) Tested Vertical Travelers

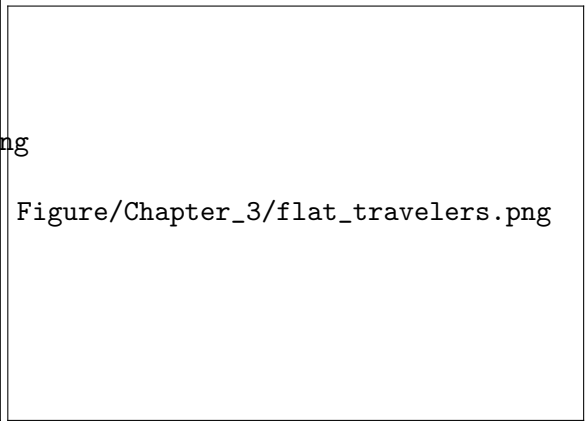

(b) Tested Flat Travelers

Figure 3.7: Tested Vertical Travelers & Flat Travelers

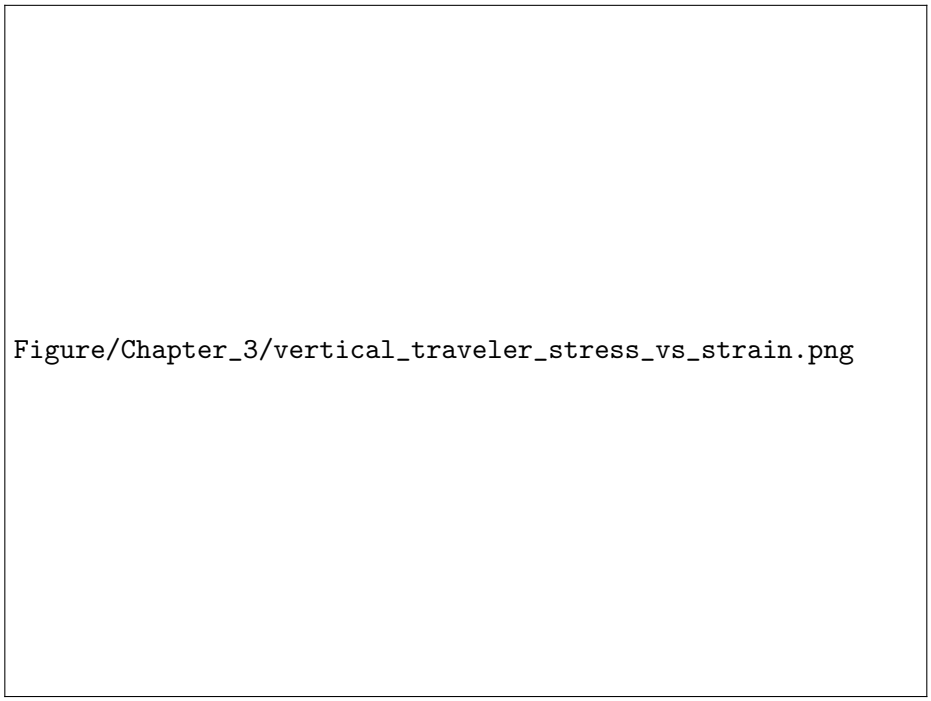

(a) Vertical Traveler

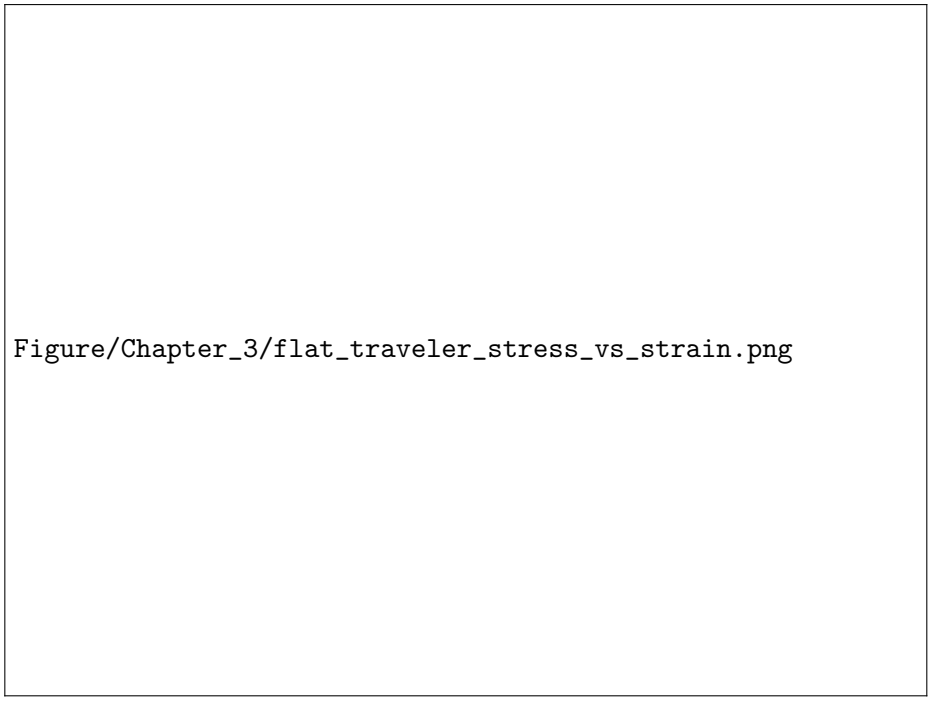

(b) Flat Traveler

Figure 3.8: Comparison of Vertical and Flat Travelers

Chapter 4

ANALYSIS

To analyze the failure mechanism of our specimen, strain data in 1 & 2 direction provides valuable insights. By plotting ϵ_{22} against ϵ_{11} as shown in Figs 4.1 & 4.4, strain behavior of the specimens before failure can be observe. Each ϵ_{22} vs ϵ_{11} plot combines the strain data from all B angle coupons. A B=0 coupon, with fibers aligned in the direction of the load, provides the maximum ϵ_{22} elongation. Conversely, a B=90 coupon, with layers aligned in the load direction, provides the maximum ϵ_{11}. It is interesting to know how would the strain of B=15, 30, 45 coupon behave in both configuration. The expectation is that the sharing of loads between fiber and layer as the angle increase will results in a lesser strain than the maximum ϵ_{22} & ϵ_{11} observed for B=0, 90. This hypothesis was verified for 0/90 configuration specimens. Consequently, determining the maximum strain for B=0 and B=90 is sufficient to establish a strain based failure criterion. As shown in Fig 4.2, if the 3D printed PEEK sustains strain equal to or exceeding the maximum strain (red dash line) of B=0, 90, failure is guaranteed. However, the ±45 configuration provides unexpected critical angle that invalidates the 0/90 failure criterion.

Experiments on ±45 configuration specimens revealed exceptional ductility compared to the 0/90 configuration specimens. The maximum ϵ_{22} for B=0 in 0/90 is approximately 10%, whereas for ±45 configuration, it is almost 70%. As shown in Fig 3.4a, both B=0 and B=15 exhibit significant strain softening before failure. The better plasticity performance of ±45 coupon in the 2-direction allows for large elongation of ϵ_{22}. Due to Poisson effect, ϵ_{11} should contract and become negative as the load is applied. Interestingly, after being negative in the elastic region, ϵ_{11} shifts toward positive upon yielding. In B=0, 15 specimens, the layer (1-direction) has tendency of expansion and propagation, creating a splitting effect between the printing layer at a specific gauge area location. This location, where positive strain appears, is denoted as HOTSPOT. HOTSPOT is observed in full field strain using DIC

software as the load is applied. Anywhere outside of the HOTSPOT, rest stays as negative strain. Full field strain images with HOTSPOT are shown in Fig 4.6. In Fig 4.5, the plot shows specific coupon with HOTSPOT. Notably, 3 out of 6 B=15 ±45 specimen (#44, #46 and #47) have ϵ_{11} shifting from negative to positive. Although #45 & #23 did not reach positive ϵ_{11}, there is evident tendency to shift towards positive. However, this shift did not complete, may be because both reached their critical ϵ_{22} first. Specimens #45, #46 and #47 are at 1.586%, 2.18%, and 3.017%, respectively, where the maximum ϵ_{11} for B=90 coupon is at 1.335%. #47 extends the boundary of max ϵ_{11}, reshaping the strain-based failure criteria visually shown in Fig 4.3. In the case of ±45 configured 3D printed PEEK, HOTSPOT generated by a critical angle (B=15) sets the limit of maximum strain. If the 3D printed PEEK component experiences strain equal to or exceeding the maximum strain obtained by B=15, failure of this anisotropic component is guaranteed.

Figure 4.1: $\epsilon 22$ vs $\epsilon 11$ (0/90)

Figure 4.2: $\epsilon 22$ vs $\epsilon 11$ max strain boundary(0/90)

Figure 4.3: $\epsilon 22$ vs $\epsilon 11$ extended max strain boundary(± 45)

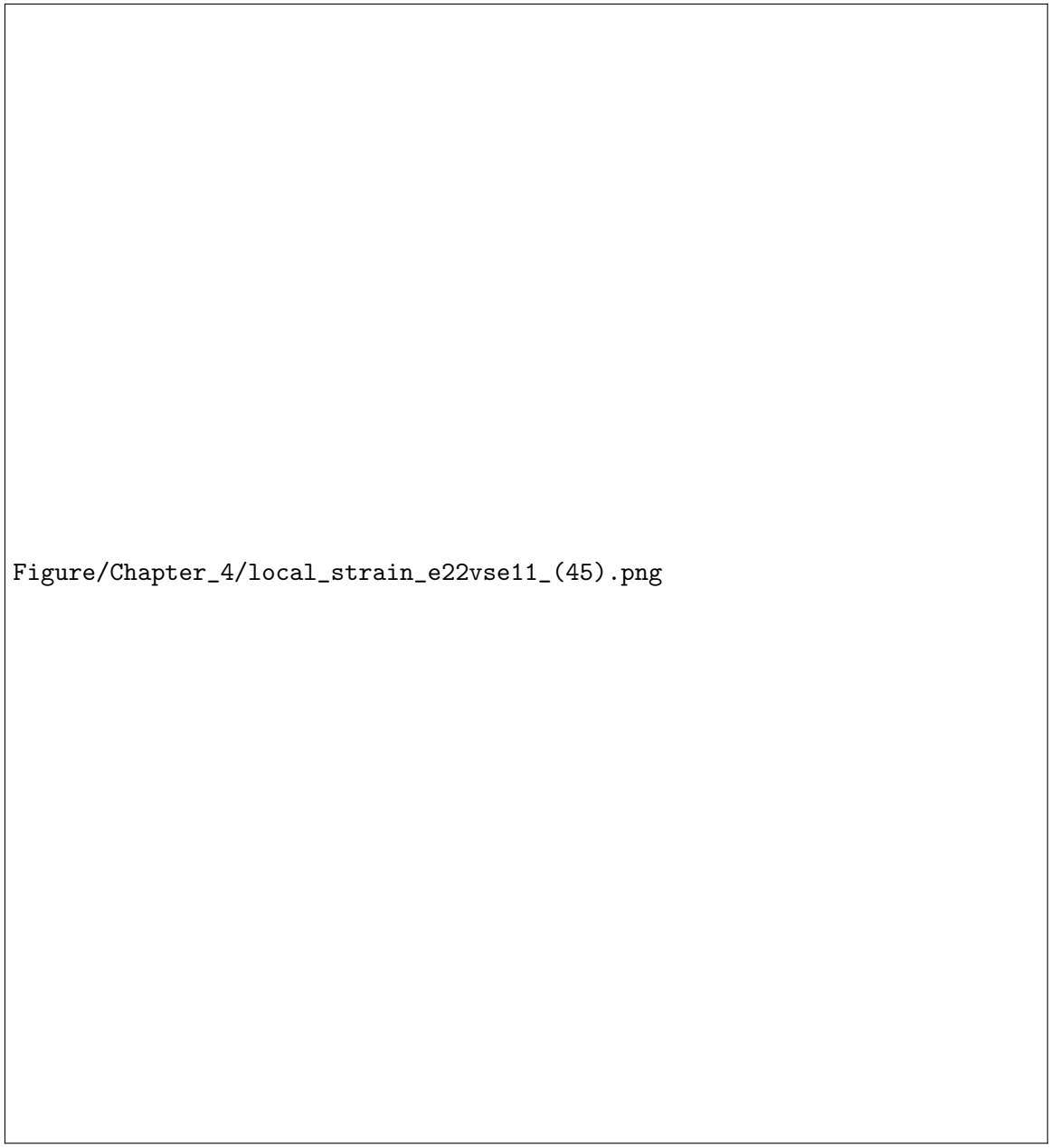

Figure 4.4: $\epsilon 22$ vs $\epsilon 11$ (± 45)

Figure 4.5: Hotspot B=0 & B=15 $\epsilon 22$ vs $\epsilon 11$

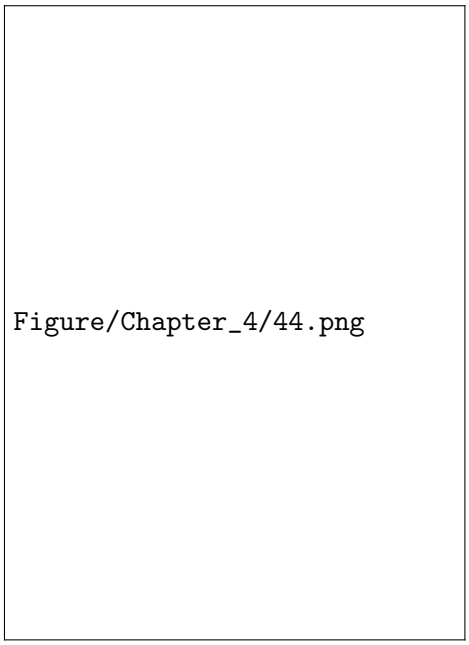

(a) #44

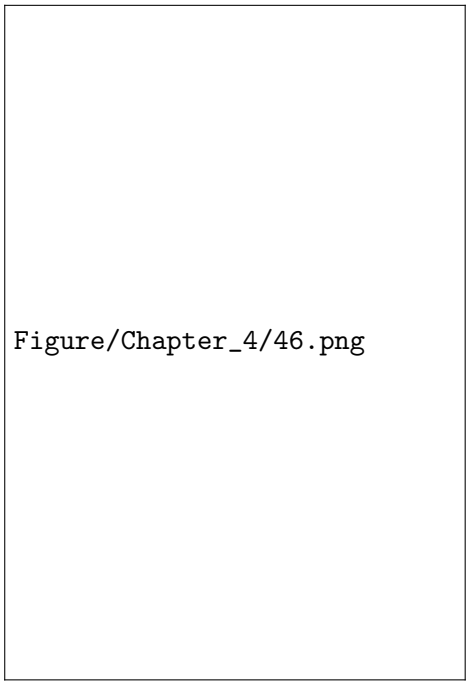

(b) #46

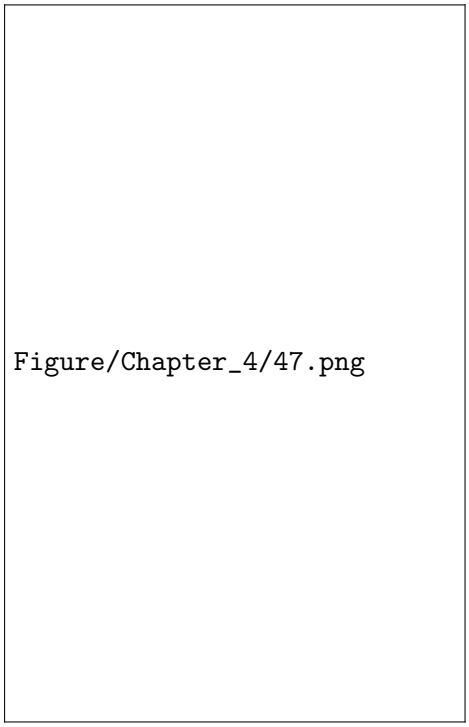

(c) #47

Figure 4.6: B=15 HOTSPOT (±45 configuration)

Chapter 5

CONCLUSION AND FUTURE WORK

5.1 Conclusion

This research explores the anisotropic behavior of 3D printed parts using Material Extrusion(MEx) 3D printing technology, a promising future manufacturing method for aerospace industry. Specimens were produced using a low-cost 3D printer to manufacture high-performance polymer (PEEK) test specimens. The preparation of these specimens involved several steps, including routing, end-tabbing ,and DIC speckling. The specimens were orientated at B= 0, 15, 30, 45, 90 angles and then experimentally tested to investigate fiber and layer interaction, as well as anisotropy, material properties suitable for Transversely Isotropic FEA model. The Digital Image Correlation (DIC) technique, which analyzes full field strain data through images captured by a high definition camera, was employed to establish a strain-based failure criterion. This criterion examined both raster configurations (0/90, ±45). It was observed that the critical strain of 0/90 configured specimen depends on the maximum ϵ_{22}=10.7% obtained at B=0 and the maximum ϵ_{11}=0.9% obtained at B=90. Interestingly, the critical strain of ±45 configured specimen depends solely on the maximum ϵ_{22}=69% & ϵ_{11}=3% obtained at B=15, where HOTSPOT occurs.

Due to porosity, inter-filament voids, and potential imperfections in the 3D printing process, a component may fail before reaching the maximum strain in any direction. Consequently, this strain-based failure criterion does not provide perfectly accurate maximum strain values, and statistical variations may occur. However, it can still serve as valuable guidance for future structural design.

5.2 Future Work

In the future, the mechanical properties obtained from this research should be used to develop a Finite Element Analysis (FEA) model. The development of the FEA model is

crucial because, once validated, it can be applied to more complex components to predict strain-based failure. If the maximum strain of a complex component, analyzed under a designed load using the FEA model, exceeds the critical strain determined in this research, the component is likely to fail under the designed load in real-world conditions.

Beyond future computational analysis, investigating different materials such as PEKK using the methodology developed in this research is highly valuable. PEKK, another high-performance material widely used in the aerospace industry, shares similar characteristics with PEEK but has minor differences that merit investigation.

BIBLIOGRAPHY

[1] AON3D. Peek – best 3d printing temperatures to maximize crystallinity, 2021. Accessed: 2024-07-02.

[2] ASTM. Standard test method for tensile properties of plastics. Designation: D638.38935.

[3] ASTM. Standard terminology for additive manufacturing—coordinate systems and test methodologies, 2019. Designation: D52921-13.

[4] Ever J Barbero. *Introduction to composite materials design*. CRC press, 2010.

[5] Ian Gibson, David W Rosen, Brent Stucker, Mahyar Khorasani, David Rosen, Brent Stucker, and Mahyar Khorasani. *Additive manufacturing technologies*, volume 17. Springer, 2021.

[6] instron. 6800 series.

[7] INSTRON. Instron accessories catalog - 8th edition, 2023.

[8] INTAMSYS. Intamsys i funmat ht i desktop 3d printer, 2022.

[9] Austin Lee, Mathew Wynn, Liam Quigley, Marco Salviato, and Navid Zobeiry. Effect of temperature history during additive manufacturing on crystalline morphology of peek. *Advances in Industrial and Manufacturing Engineering*, 4:100085, 05 2022.

[10] Todd Letcher and Megan Waytashek. Material property testing of 3d-printed specimen in pla on an entry-level 3d printer. In *ASME international mechanical engineering congress and exposition*, volume 46438, page V02AT02A014. American Society of Mechanical Engineers, 2014.

[11] Arlene Lo. Hexcel makes boeing's qualified provider list for 3d printed aircraft components, 2019.

[12] Partha Modak, Md Hossain, Md Imtiaz Ikram, and S. Ahmed. A comparative analysis of elastostatic responses of a cross-ply and angle-ply laminated panel using a single-variable lamination theory. *Procedia Engineering*, 90, 12 2014.

[13] shorewestern. 306 series loadframes.

[14] ultimaker. Ultimaker cura, 2024.

[15] Timothy Yap, Nathaniel Heathman, Tim Phillips, Joseph Beaman, and Mehran Tehrani. Additive manufacturing of polyaryletherketone (paek) polymers and their composites. *Composites Part B: Engineering*, 266:111019, 2023.

[16] ZEISS. Zeiss inspect the metrology software for all challenges, 2024.

[17] ZUND. G3 digital cnc cutter, 2024.

Appendix A

TEST PLAN SCHEMATIC

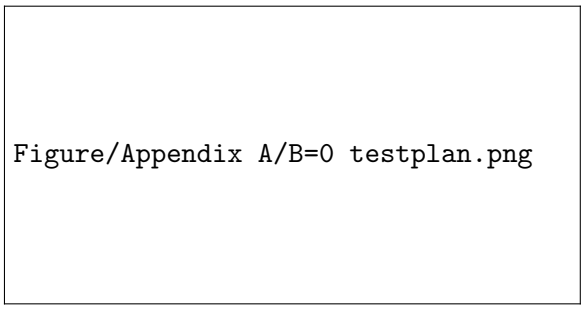

(a) B=0

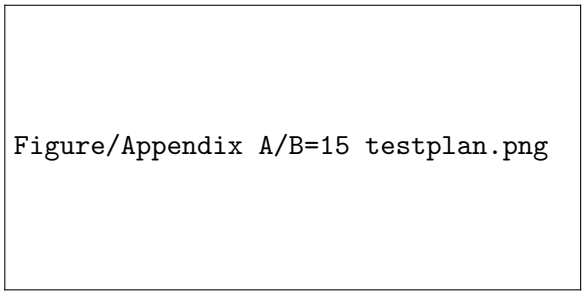

(b) B=15

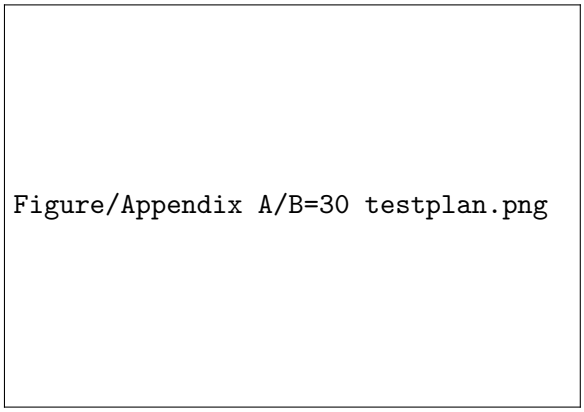

(c) B=30

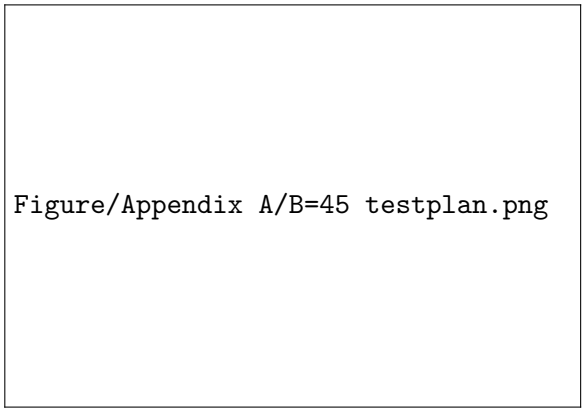

(d) B=45

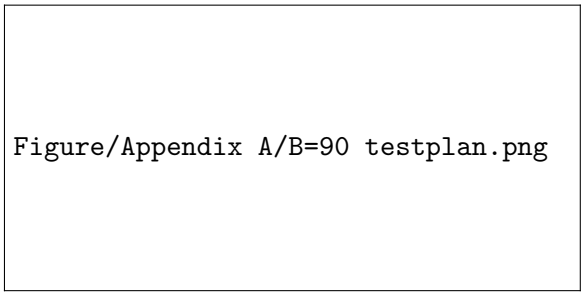

(e) B=90

Figure A.1: Test Plan Schematic

Appendix B

MATLAB CROP AND BW CODE

```
3%%
clear; clc; close all
imfile = 'file_location';
f = dir([imfile, '\*.jpg']);
mkdir([imfile,' Cropped BW']);
cd([imfile,' Cropped BW']);
im = imread(strcat(f(1).folder,'\',f(20).name));
rot = 0.;
im = imrotate(im,rot,'bilinear','crop');
[j,rect] = imcrop(im);
%im=imadjust(im,[0.5,0.55],[]);
%im=blendexposure(im,im,'Contrast',0.5);
close all
%%
parfor ii = 1:length(f)
    im = imread(strcat(f(ii).folder,'\',f(ii).name));
    im = imrotate(im,rot,'bilinear','crop');
    %im= imadjust(im,[0.5,0.55],[]);
    %im= blendexposure(im,im,'Contrast',0.5);
    im = imcrop(im,rect);
    imbw = rgb2gray(im);
    imwrite(imbw,f(ii).name)
end
disp('Done')
```

Listing B.1: MATLAB Crop and Black & white code by Troy Nakagawa